Nonlinear Processes in Geophysics (1999) 6: 195–204

Nonlinear Processes in Geophysics

Polar spacecraft observations of the turbulent outer cusp/magnetopause boundary layer of Earth

J. S. Pickett, J. D. Menietti, J. H. Dowell, D. A. Gurnett, and J. D. Scudder

Department of Physics and Astronomy, The University of Iowa, Iowa City, IA 52242-1479, USA

Received: 18 May 1999 – Accepted: 16 July 1999

Abstract. The orbit of the Polar spacecraft has been ideally suited for studying the turbulent region of the cusp that is located near or just outside the magnetopause current sheet at 7-9 R_E. The wave data obtained in this region show that electromagnetic turbulence is dominant in the frequency range 1-10 Hz. The waves responsible for this turbulence usually propagate perpendicular to the local magnetic field and have an index of refraction that generally falls between the estimated cold plasma theoretical values of the electromagnetic lower hybrid and whistler modes and may be composed of both modes in concert with kinetic Alfvén waves and/or fast magnetosonic waves. Fourier spectra of the higher frequency wave data also show the electromagnetic turbulence at frequencies up to and near the electron cyclotron frequency. This higher frequency electromagnetic turbulence is most likely associated with whistler mode waves. The lower hybrid drift and current gradient instabilities are suggested as possible mechanisms for producing the turbulence. The plasma and field environment of this turbulent region is examined and found to be extremely complex. Some of the wave activity is associated with processes occurring locally, such as changes in the DC magnetic field, while others are associated with solar wind and interplanetary magnetic field changes.

1 Introduction

Since its launch in February 1996, the Polar spacecraft has made several passes through a very turbulent region located in the earth's cusp and near the outer cusp's boundary with the magnetopause (usually about 7-9 R_E). This region is best characterized by large fluctuations in the magnetic field. We believe this region to be the same as that termed the turbulent boundary layer (TBL) by Savin et al. (1998) based on similar turbulent magnetic field data taken onboard the Interball Tail probe. They state that this layer lies in the cusp just outside the main magnetopause current sheet, the point at which the magnetic field turns from earth-controlled to magnetosheath-controlled according to Haerendel and Paschmann (1975). Savin et al. (1998) state that the magnetopause current sheet is deflected from the model magnetopause to a depth of 1-2 R_E into the cusp (see Fig. 1 of Savin et al., 1998). The TBL is generally differentiated from the outer cusp throat and magnetosheath by its much higher ion temperatures. We adopt the term TBL for the remainder of this paper since it aptly describes the particular region under study.

Very few spacecraft have sampled this turbulent region of the high latitude cusp for such long periods of time as has Polar. Most spacecraft just pass through the TBL region within a few tens of minutes during their inbound and outbound passes through the bow shock and magnetopause regions. During some orbits, Polar remained in this turbulent region for a few hours since it was traveling across the region at its apogee, rather than passing through it. Those spacecraft that have made measurements in this region did not carry nearly the sophisticated complement of instrumentation and/or obtain nearly as high time resolution data as Polar. Hawkeye-I (Gurnett and Frank, 1978), ISEE-1 and ISEE-2 (Gurnett et al., 1979), Prognoz-10 (Klimov et al., 1986), AMPTE/IRM (Labelle and Treumann, 1988), and Prognoz-8 (Blecki et al., 1998), to name just a few, have obtained data in this region and near the magnetopause in general showing the turbulent electric and magnetic fields. None of them were able to state with certainty the wave mode of the turbulence or its generation mechanism.

Due to the turbulent nature of the TBL region, it is expected that nonlinear processes will occur in it. Below we present evidence of nonlinear plasma wave turbulence from a representative TBL through measurements obtained by the Polar spacecraft. In order to better understand the role of the observed waves, we also provide some particle and field data, as well as supporting solar wind and interplanetary magnetic field (IMF) data. Following this introduction are a description of the instrumentation, a review of some of the observations made in the TBL and an analysis of those observations,

Correspondence to: J. S. Pickett

a discussion of these results and the conclusions drawn from the analysis and discussion. This study is being carried out under the auspices of the International Solar-Terrestrial Physics (ISTP) and Global Geospace Science (GGS) programs through the U. S. National Aeronautics and Space Administration with the aim of understanding sun-earth global processes through the use of observations (multi-spacecraft and ground-based), modeling and theory (Acuna et al., 1995).

2 Instrumentation

The wave electric and magnetic field data used in this study were obtained by the GGS-Polar Plasma Wave Instrument (PWI) (Gurnett et al., 1995), the particle data were obtained by the GGS-Polar Hydra instrument (Scudder et al., 1995), the magnetic field data were obtained by the GGS-Polar Magnetic Field Experiment (MFE) (Russell et al., 1995), and the spacecraft potential data were obtained by the GGS-Polar Electric Field Instrument (EFI) (Harvey, et al., 1995). The Polar spacecraft (Fig. 1) was launched on February 24, 1996, and placed into an ~ 1.8 by 9.0 R_E orbit with an inclination of about 86 degrees (putting apogee initially over the northern polar region) and orbit period of about 18 hours. This orbit was ideally suited for studying the earth's northern cusp at radial distances of 7 to 9 R_E. The main body of the spacecraft had a spin rate of approximately 6 rpm in order to obtain waves, fields, and particle measurements while the despun platform on top of the main body contained imaging instruments.

PWI carried 5 different receivers, two of which sampled the frequency domain and were used primarily for surveying the data, and three of which sampled the time domain and were ideal for studying microphysics. Most of the results reported here are obtained through analysis of the Low Frequency Waveform Receiver (LFWR), which obtained waveforms every 18 or 28 seconds, depending on the mode. These waveform snapshots covered a total time of 4.64 or 2.56 s, respectively, and were sampled at the rate of 100 samples per second. The LFWR contained a bandpass filter that rolled off steeply below 1 Hz and above 25 Hz. All six channels (three each orthogonal electric and magnetic antennas) were sampled simultaneously. This allowed us to obtain the Poynting vector directly since two of each of the electric and magnetic searchcoil antennas (E_U, E_V, B_U, B_V as seen in Fig. 1) made orthogonal measurements in the spin plane, and the remaining two (E_Z, B_Z as seen in Fig. 1) made measurements along the spin axis. The triaxial searchcoil was located on the end of a 10 m boom. The electric measurements were made by double probe antennas, 130 m and 100 m tip-to-tip along the U and V directions, respectively, in the spin plane, and 14 m along the Z direction or spin axis. The LFWR data were processed by a high rate processor and stored on a tape recorder until telemetered to a ground station. The LFWR data were calibrated in amplitude and phase by using the calibration data at 7 Hz. This frequency was chosen because it lies near mid-frequency range of the observed turbulence.

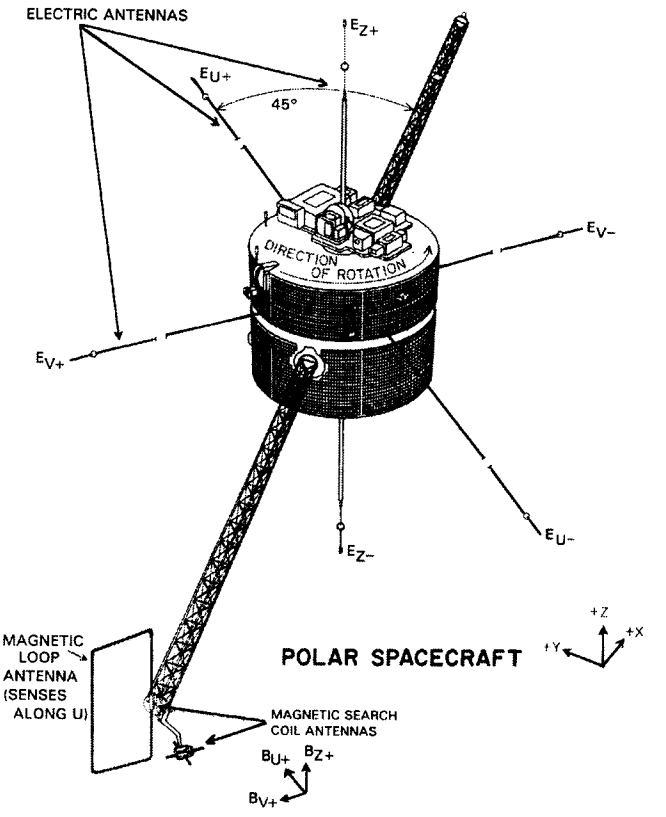

Fig. 1. A view of the Polar spacecraft showing the various electric and magnetic antennas.

In addition to the LFWR, we present results from the PWI Multichannel Analyzer (MCA). The MCA had a pair of analyzers which generally continuously sampled one electric (E_U) and one magnetic (B_U) antenna. The MCA sampled in the frequency domain with parallel filtering and detection channels. A spectrum was obtained every 1.3 s in the frequency range of 5 Hz to 311 kHz for E_U and 5 Hz to 10 kHz for B_U, with all channels being sampled simultaneously for each analyzer.

The Hydra instrument provides total fluxes of electrons and ions in three dimensions over the energy range of ~2 keV/e - 20 keV/e with a full electron or ion spectrum being produced every ~ 2.3 s. The MFE instrument provides 3-axis DC magnetic field measurements with a sampling rate of 108 Hz through the Hydra data stream. EFI contributes a moderately high time resolution spacecraft potential which is for the most part an indication of the thermal electron density (Pedersen, 1995).

3 Observations and Analysis

3.1 Wave observations from the Polar spacecraft

Pulse-type waveforms (bipolar and monopolar) are occasionally observed in the LFWR data. Figure 2 presents an example of such a pulse obtained on September 11, 1996, when the

Polar spacecraft was in the TBL region described in the introduction. The radial distance of the spacecraft, R_E, the magnetic L-shell, L, the magnetic latitude, λ_m, and Magnetic Local Time, MLT, for this snapshot are shown at the bottom of the plot. This example shows a pulse centered at approximately 01:41:22.4 UT which lasts approximately 140 ms. Panels 3-5 show amplitude of the measured electric field components in mV/m in the range 1 to 25 Hz along the vertical axis and time on the horizontal axis. The bottom three panels (6-8) show the amplitude of the measured magnetic field components in nT for the same frequency range and time. The data are presented in a local **B**-field aligned coordinate system determined by measurements taken on Polar by the MFE instrument in which the Z axis (panels 5 and 8) is parallel to the local magnetic field, $\mathbf{B}_0$, the X axis (panels 3 and 6) is chosen so that the radial vector outward from the center of the earth to the spacecraft location, **R**, is in the meridian plane (contained in the north-south, or X-Z plane), and Y (panels 4 and 7) completes the right-handed coordinate system, being generally in the eastward direction. Both the X and Y directions are perpendicular to $\mathbf{B}_0$.

We note that the pulse at 01:41:22.4 UT in Fig. 2 has its electric components primarily contained in the plane perpendicular to $\mathbf{B}_0$ with the $E_{Y\perp}$ component having the largest amplitude of about 6 mV/m peak-to-peak. The pulse's magnetic components, on the other hand, are not totally confined to either the parallel or perpendicular directions. However, the largest component appears to be parallel to $\mathbf{B}_0$, $B_{Z//}$, with an amplitude of about 3.5 nT peak-to-peak. In this coordinate system only the $B_{Z//}$ component appears bipolar with the rest of the components being nearly monopolar. As mentioned above, the remainder of the snapshot in Fig. 2 shows fluctuations characteristic of turbulence in both the wave electric and magnetic fields with few, if any, isolated pulses or sinusoidal wave trains. In this region of space the LFWR waveforms typically resemble turbulence, but with occasional isolated pulses and bursty, near sinusoidal wave trains.

The second panel of Fig. 2 shows the magnitude of the local magnetic field with its scale, in nT, on the left vertical axis and the lower hybrid frequency, f_{LH}, with its scale, in Hz, on the right vertical axis. In this frequency range, f_{LH} is equal to $(f_{cp} f_{ce})^{1/2}$, where f_{cp} (~ f_{ce}/1837) and f_{ce} (~ 28 |**B**|) are the measured proton and electron cyclotron frequencies, in Hz, respectively. For reference, f_{LH} usually falls within the frequency band, 1-25 Hz, of the LFWR, with f_{cp} falling below the lower limit of this frequency band and f_{ce} falling well above the band's higher limit during times when Polar is in the TBL regions. At the time of the pulse seen at 01:41:22.4 UT, f_{LH} ~ 14 Hz.

The top panel of Fig. 2 shows the index of refraction, n, for the entire time period, where n is equal to c|**B**|/|**E**|, c is the speed of light, |**B**| is the magnitude of the wave magnetic field vector and |**E**| is the magnitude of the wave electric field vector as measured by the LFWR . During the pulse, n spikes up to ~2000 from a level of around 200-600, but then settles down to about 15-20. The spike and subsequent low level of n are caused by the highest amplitudes of the magnetic

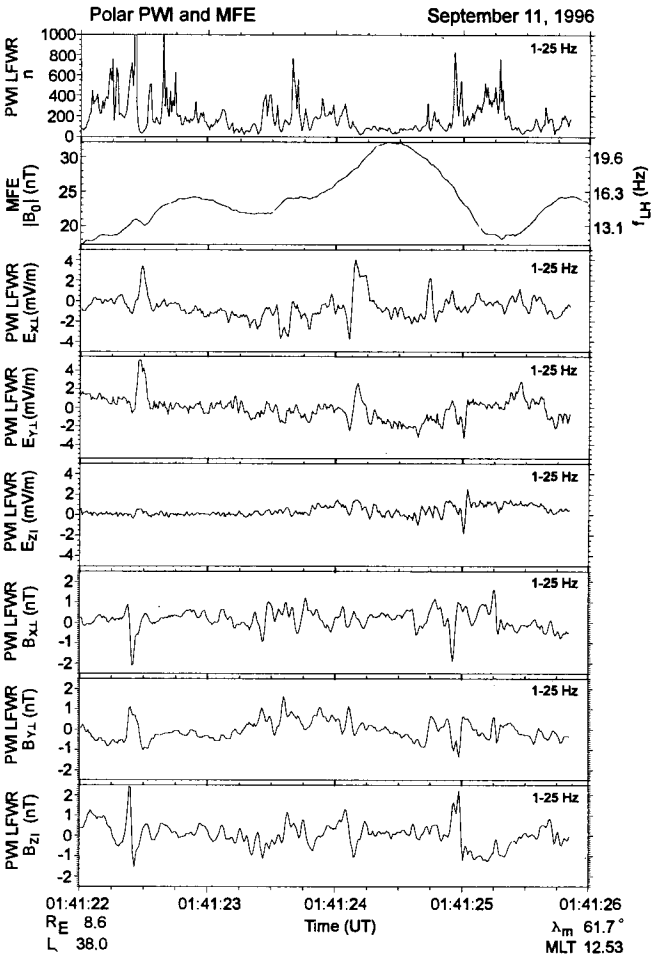

Fig. 2. Four-second plot of the index of refraction, magnetic field, and 6 components of the AC waves in a local **B**-field aligned coordinate system in the frequency range 1-25 Hz showing the turbulent nature of the waves. The lower hybrid frequency has been provided in panel 2 with its scale on the right-hand side. Note the pulse at 01:41:22.4 UT.

components arriving before those of the electric components. We have found that this is often the case. For the remainder of the snapshot we observe primarily turbulence with varying degrees of n. For the most part, aside from the spikes, the measured index of refraction generally falls into the range of 50-300.

For whistler mode waves propagating along **B**, the index of refraction squared is $n^2 \approx f_{pe}^2 / f f_{ce}$, where f_{pe} is the electron plasma frequency in Hz. Using our values of f_{ce} = 588 Hz based on MFE data, f_{pe} = 28.5 kHz based on Hydra data, and f = 7.1 Hz based on the duration of the pulse as 140 ms, we obtain n = 441. This value appears to be above or close to the measured value of n during the first part of the pulse (ignoring the spike), but approximately 30 times too large in the latter part where the electrostatic components dominate. The estimated whistler mode index of refraction of 441 seems to be above the upper limit of the measured n range during most of the rest of the turbulence. For whistler mode waves propagating near the resonance cone (oblique wave normal angles), the calculated value for n would be even larger by about a

factor of 2 for angles with respect to **B** around 75° and by a factor of 100 and greater for angles of 89-90°. For electromagnetic lower hybrid waves, Thejappa et al. (1995a) have derived the index of refraction as $n = (\omega_{pe} / \omega_{ce})(\omega_{pe} / kc)$ where ω_{pe} and ω_{ce} are the electron plasma and cyclotron frequencies in rad/s, respectively, and k is the wavenumber. Since none of PWI's receivers are in interferometry mode at this time, we do not measure k, which is equal to $2\pi/\lambda$, λ being the wavelength. Hence, our only recourse for this time period is to use an estimate of the lower limit of λ based on an analysis done by Gurnett et al. (1979) for obtaining the wavelength of turbulence observed at the magnetopause on ISEE 1 and ISEE 2. Their analysis showed that the wavelengths of the turbulence below 10 kHz must be at least as large as 215 m based on the antenna length and other factors. Using this number for λ, $k = 2.92 \times 10^{-2}$ m^{-1}, and using the above equation for the index of refraction derived by Thejappa et al. (1995a), we calculate $n \sim 1$ for electromagnetic lower hybrid waves. Most likely the wavelength is much longer than this, thus pushing n up to values which could fall into the lower range of the measured values for n. In fact, if we take the equation for the calculation of the index of refraction for the electromagnetic lower hybrid mode, use our values for measured n of ~ 200, and f_{ce} and f_{cp} as above, we obtain a value for k of 1.45×10^{-4} m^{-1}. This value is extremely close to the value of k determined by Thejappa et al. (1995a) for 9 Hz waves in their study of low-frequency electromagnetic waves associated with Langmuir waves in the solar wind. They identified the low frequency waves as electromagnetic lower hybrid waves and proposed that they arose from currents associated with gradients in the electron beam originating at sites where Langmuir waves scatter the beam electrons. They also state that if the ratio E/B of the waves is less than the electron thermal speed, the waves would be heavily Landau damped if they were purely electromagnetic waves, thus eliminating ordinary whistlers with wave vector along the magnetic field. For the pulse at 01:41:22.4 UT, the electron thermal speed is around 4.1×10^3 km/s based on Hydra data and our E/B ratio determined from the index of refraction obtained above was $1.0\text{-}1.5 \times 10^3$ km/s for most of the pulse. Thus, E/B is less than the electron thermal speed and we can probably rule out the whistler mode for much of the turbulence.

We assume that the pulses represent a single-event or an elementary entity of turbulence, i.e., an early stage of the turbulence before it has evolved to the more typical chaotic state, and thus they can provide us with a reliable wave mode. Under this assumption, we proceed by obtaining the wave normal angle and Poynting vector. In order to obtain the wave normal angle, we use the minimum variance method (Sonnerup and Cahill, 1967) to transform the **B**-field aligned, 3-component LFWR wave magnetic field components into a principal axis system. In this system, the eigenvector corresponding to the smallest eigenvalue computed from the minimization of the standard deviations of the LFWR wave magnetic field components is the wave normal vector. The eigenvectors corresponding to the largest and medium eigenvalues contain the plane perpendicular to the wave normal

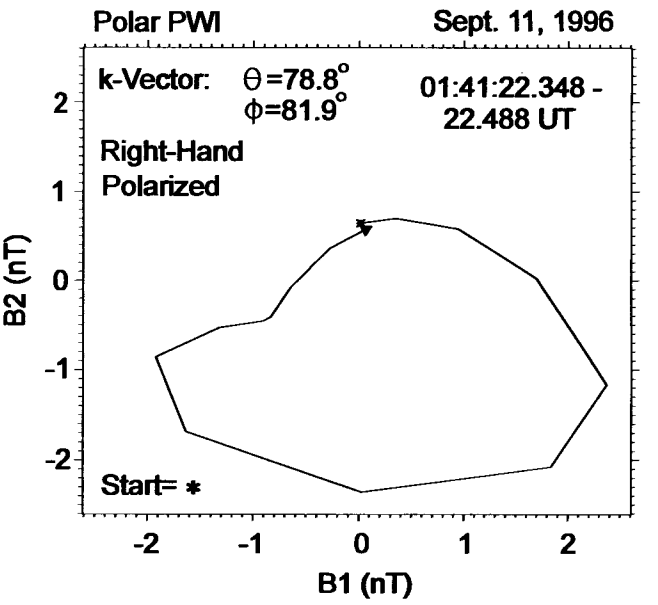

Fig. 3. Plot of the pulse from Fig. 2 in the plane perpendicular to the wave normal vector, with the largest eigenvector magnitudes, B1, plotted vs. the medium eigenvector magnitudes, B2. One revolution about the wave normal is completed in 140 ms.

vector, which is defined as the plane of polarization. The hodogram shown in Fig. 3 for the pulse identified in Fig. 2 at 01:41:22.4 UT is a plot of the largest, B1, vs. the medium, B2, values of the transformed LFWR magnetic components in the principal axis system using the minimum variance analysis method, and thus represents the rotating magnetic field of the wave in the plane perpendicular to the wave normal. Fig. 3 shows that the pulse completes one revolution in this plane in about 140 ms (corresponding to the 14 samples over which the analysis was performed), the polarization has been determined to be right-handed and somewhat elliptical, and the wave normal angle, θ, with respect to $\mathbf{B}_0$ has been determined to be 78.8°. Furthermore, the time average Poynting vector ($\langle \mathbf{S} \rangle = (1/\mu_0)(\mathbf{E} \times \mathbf{B})$), where μ_o is the permeability constant and **E** and **B** are the measured wave electric and magnetic field vectors, was determined to have an angle, θ_S, with respect to **B** of 113.1° and magnitude of 1.7×10^{-6} W/m^2.

In order to find out if the large amplitude turbulence takes place in density cavities or during large gradients of **B**, we have plotted in Fig. 4 from top to bottom: the negative of the spacecraft potential from EFI, the PWI LFWR electric X component in the GSM system, the PWI LFWR magnetic X GSM component, and the X,Y,Z components of the DC-54 Hz **B**-field in GSM coordinates. There are two main points to gather from this plot: 1) the large amplitude fluctuations in the AC magnetic field appear to be more closely tied with gradients of **B**, and 2) the large amplitude fluctuations observed only in the electric components appear to be associated with density changes, i.e., at t = 01:41:24.2, where the potential is a minimum. This last point is somewhat questionable because the spacecraft potential is undersampled.

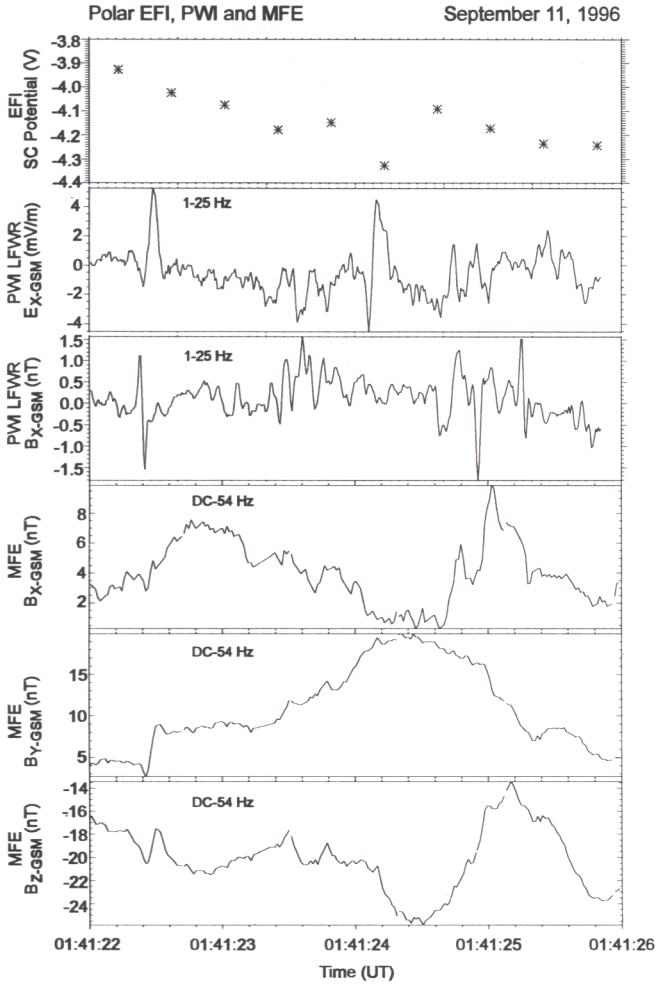

Fig. 4. Four-second plot of the negative of the spacecraft potential, one component of each of the AC electric and magnetic waves in the 1-25 Hz range, and 3 components of the DC-54 Hz magnetic field, all in the GSM coordinate system covering the same time period as Fig. 2.

We have presented all of our data thus far in the time domain since the typical method for obtaining a frequency domain spectrum is through application of a Fourier transform. Transforming the isolated pulse and turbulence to the frequency domain with a windowed Fourier transform, WFT, leads to broadband and broadband with harmonic structure spectra, respectively, which give an inaccurate description of the waves. This is the case because the WFT imposes a scale or response interval T into the analysis. The inaccuracy arises from the aliasing of high- and low-frequency components that do not fall within the frequency range of the window (Torrence and Compo, 1998). Thus, we have resorted to wavelet analysis to decompose our data into time-frequency space because it is capable of analyzing time series that contain nonstationary power at many different frequencies, such as impulsive or turbulent data. We have used the Morlet wavelet function, which consists of a plane wave modulated by a Gaussian, because it has zero mean and is localized in both time and frequency space. Furthermore, it is nonorthogonal which means it is useful for time series analysis, where

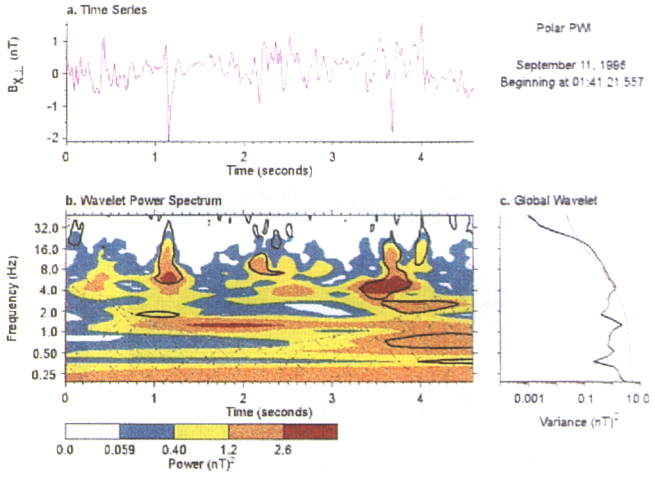

Fig. 5. (a) Time series of the LFWR $Bx_{\perp}$ component of the 1-25 Hz waves in the **B**-field aligned coordinate system, (b) the wavelet power spectrum. The contour levels are chosen so that 75%, 50%, 25%, and 5% of the wavelet power is above each level, respectively. Cross-hatched region is the cone of influence, where zero padding has reduced the variance. Black contour is the 10% significance level, using the global wavelet spectrum as the background. (c) The global wavelet power spectrum (black line). The red dashed line is the 10% significance level for the global wavelet spectrum, assuming a white-noise background.

smooth, continuous variations in wavelet amplitude are expected. On the other hand, the results at large scales (low frequency), where the wavelet spectrum at adjacent times is strongly correlated, is highly redundant. For more information on the use of wavelets in geophysics, see Torrence and Compo (1998). A plot of the LFWR $B_{x\perp}$ waveform data from Fig. 2 and its corresponding wavelet transform are shown in Fig. 5. Here we see that the isolated pulse contains most of the power at the time it was observed (Fig. 2b) and that its frequency as seen by the contour outlined in black is centered around 7 Hz. This agrees with our analysis above where we found that the wave pulse completed one rotation around the wave normal direction in 140 ms. Additionally we note that there are two other contours with high degrees of confidence that contain significant power in the frequency range ~ 3-10 Hz. All of these thus occur at frequencies below f_{LH} (~11-21 Hz, see Fig. 2), with nearly zero power for waves above f_{LH}. Most of the power observed below 1 Hz is not valid due to the filter rolloff at this frequency and for the reason described above with regard to nonorthogonal wavelet functions. Therefore, the valid range of frequencies is 1 Hz to 25 Hz, the upper rolloff of the filter. The global wavelet spectrum shown in Fig. 5c is the time average over all of the local wavelet spectra shown in Fig. 5b. It may provide an unbiased and consistent estimation of the true power spectrum of a time series, and a useful measure of the background spectrum against which peaks in the local wavelet spectra could be tested. We have examined the other five components using wavelet analysis, including the three electric components, and have found the same results, i.e., most of the wave power falls in the frequency range of 3-10 Hz.

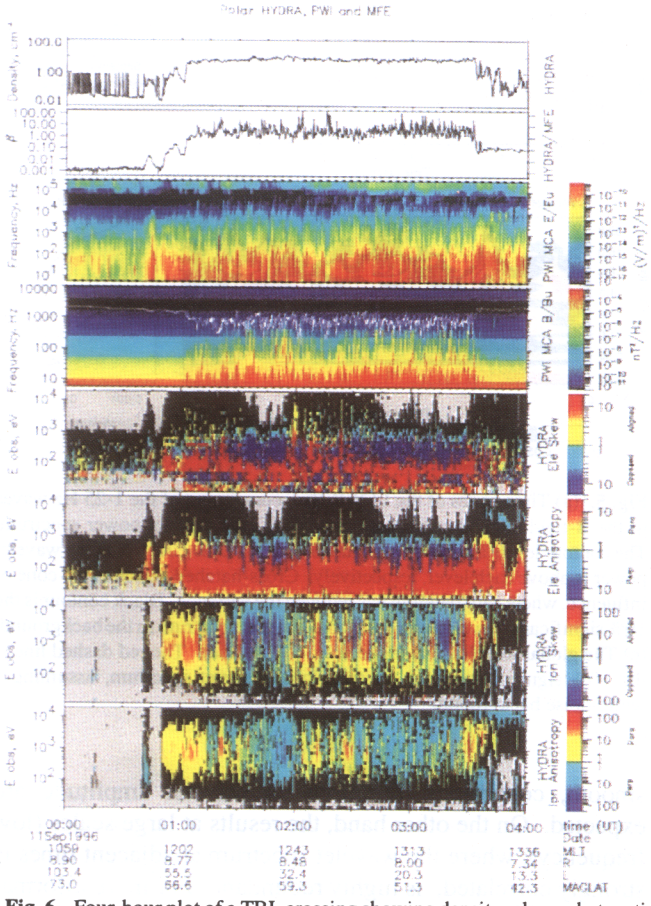

Fig. 6. Four-hour plot of a TBL crossing showing density, plasma beta ratio of total particle pressure to magnetic pressure, AC electric and magnetic waves in the range 5 Hz to 311 kHz and to 10 kHz, respectively, the electron skew and anisotropy, and the ion skew and anisotropy. Note that the white line in panel 4 is the electron cyclotron frequency calculated from the measured magnetic field. Skew plots show the difference between field-aligned and field-opposed fluxes at fixed energy. "Warm" colors (yellow and red) indicate net flux in the B field-aligned direction, and "cold" colors (cyan and blue) indicate net flux in the opposed direction. Black indicates that there is no experimentally significant difference between the measurements. Grey indicates that a useful calculation could not be performed. Skew is made dimensionless by dividing by the expected Poisson and other errors in the fluxes compared. For electrons skew corresponds to the pear-shapedness of $f_e(V)$ and is a remnant of a conductor. For ions, skew corresponds to flow asymmetries and conduction, but primarily flow. Anisotropy shows the difference between aligned and perpendicular spectra. Field-aligned and field-opposed spectra are averaged (with equal weights) and compared to the perpendicular spectrum, again in units of the expected error.

In these TBL regions, several other types of waves are typically observed. Electromagnetic broadband waves are often seen in the MCA data with the magnetic components extending up to about f_{ce}, an example of which is provided in Fig. 6 and discussed below. Extremely bursty (few seconds or less) electromagnetic, right-hand polarized, weak oscillatory waves are occasionally observed by the LFWR at frequencies around $f \approx 2\ f_{LH}$ during times when the magnetic field is extremely depressed (around 10-15 nT) and the low frequency wave electric field is so low that these bursty waves are not even resolved by the LFWR. Similar bursts are observed by PWI's higher frequency receivers at frequencies of a few hundred Hz and just below f_{ce}. Also at higher frequencies electron cyclotron harmonic waves are observed with the fundamental frequency at or just above f_{ce} and often with several (> 3) harmonics. Electrostatic solitary structures are observed throughout the TBL and various regions of the magnetosphere (cf. Franz et al., 1998; Cattell et al., 1999). When their waveforms, which resemble bipolar and monopolar pulses, are transformed to the frequency domain via an FFT, the typical broadband spectrum results, thus the name broadband electrostatic noise (BEN).

3.2 A representative TBL crossing by the Polar spacecraft

In order to gain a better understanding of the region in which the electromagnetic turbulence is observed, we need to review several of the other Polar measurements. Fig. 6 is a 4-hour plot of various Polar measurements during Polar's transit of the TBL on September 11, 1996 (from which the LFWR snapshot shown in Fig. 2 was taken). The spacecraft was in the TBL from about 0100 to 0340 UT, corresponding to a range in MLT from 12 hrs. to 13.5 hrs. at a radial distance of from 8.8 to 7.2 R_E and in the magnetic latitude range of 67 to 45°. Immediately obvious in panel 4 is the fact that during this entire time the local DC magnetic field (based on the white line trace of f_{ce}) was depressed and extremely noisy, the density (panel 1) was nearly steady around 10 cm^{-3} and the plasma beta ($p/(B^2/2\mu_0)$, where p is the total particle pressure, B is the magnitude of the magnetic field, and μ_0 is the permeativity constant) generally fell within the range of 1-10 (panel 2). Furthermore, the electrons appear to be moderately anisotropic throughout much of the time period (panel 6) with the exception of near the beginning and end of the crossing where a strongly parallel population around 20-200 eV, and a slightly perpendicular component around 300-1000 eV were observed. In addition the electron skew (panel 5) shows us that the electrons are fairly well ordered in energy, being strongly aligned with the magnetic field around 30-100 eV and strongly opposed to the magnetic field around 100-1000 eV. The ions in the range 200-10000 eV/e also appear to be ordered parallel and perpendicular to $\mathbf{B}_0$ (panel 8) as well as aligned or opposed to $\mathbf{B}_0$ (panel 7) but with the ordering taking place more or less across all energies at any one time, which is in contrast to the electrons. From Fig. 6, it is clear that the TBL is a very complex region with respect to both particles and fields.

Also included for reference in Fig. 6 are the MCA wave spectra that show that the wave magnetic field (panel 4) is turbulent, up to the electron cyclotron frequency (the white trace), during the very same time period that the DC magnetic field is noisy, but the wave electric field (panel 3) is noisy before, during and after the event, with broadband waves extending from the lowest frequency measured, 5 Hz, to about 10 kHz (well above f_{ce}). This implies that these waves, historically called BEN, are distinct from the turbulence that cuts off at f_{ce}. Pickett et al. (1999) and Franz et al. (1998) show that BEN is present in this region of space, and that BEN is the result of an FFT of a bipolar pulse, and interpreted

as solitary potential structures propagating along the magnetic field. These nonlinear structures are present in the TBL along with several other types of waves mentioned above, many of which are nonlinear. Some of the solitary potential structures have been shown to be associated with ion heating (Tsurutani et al., 1998), and may, in fact, be associated with magnetic reconnection as well. Based on Viking observations of the dayside oval, Pottelette and Treumann (1998) have described the structures, BEN, as "the messengers of reconnection" occurring along the magnetic field lines which are connected to the reconnection sites at the magnetopause. Pickett et al. (1999) report that the solitary structures are seen propagating both up and down the field lines in the cusp TBL. The various properties of these solitary structures and the proposed mechanisms by which they are created are discussed elsewhere in this special issue so we will not speculate further about them other than to emphasize that they are distinctly different from the waves discussed here. The wave electric field shown in panel 3 of Fig. 6 is obviously a mixture of the solitary structures and the electric components of the electromagnetic turbulence and pulses discussed above.

Caution needs to be used in interpreting the electromagnetic turbulence observed in panel 4 of Fig. 6. Because the MCA sampled in the frequency domain, we do not have access to the waveforms. However, data from our high frequency receiver in the TBL regions have been analyzed with wavelet analysis. What we find with the magnetic components at frequencies from 20 Hz to 25 kHz is that there are no broadband waves. Rather, there are very bursty waves with little power in the frequency range of a few hundred Hz up to f_{ce}, and bursty waves with much higher power levels around 20-100 Hz. Most of these bursts are associated with waveforms that resemble turbulence. It is likely that this is whistler mode turbulence, but we cannot be certain until we complete our analysis.

3.3 Solar Wind and IMF observations from the Wind spacecraft

Figure 7 is an overview of the solar wind and IMF measurements made by the Wind spacecraft Solar Wind Experiment (SWE) and Magnetic Field Investigation (MFI), respectively, for the same time period as Fig. 6, i.e., 00:00:00 to 04:00:00 UT on September 11, 1996. During this time, Wind was about 5 R_E upstream from the bow shock of Earth and approximately 16 R_E duskward of the earth-sun line (~ 18,16,1 R_E in GSE coordinates) as it was headed northward into the earth's magnetosphere. Because of this close proximity to, and outside of, the bow shock, the solar wind delay time between Wind and Polar is at most about 2 minutes. Panels 4-6 of Fig. 7 provide the solar wind velocity components in the GSM coordinate system in km/s. The flow speed is around 540 km/s during the start of the TBL interval (01:00 to 01:35 UT) and then rises to about 580 km/s at its end. These flow speeds are somewhat typical, with most of the speed directed along the sun-earth line (X_{GSM}). However, at the point at which Polar starts to encounter the TBL

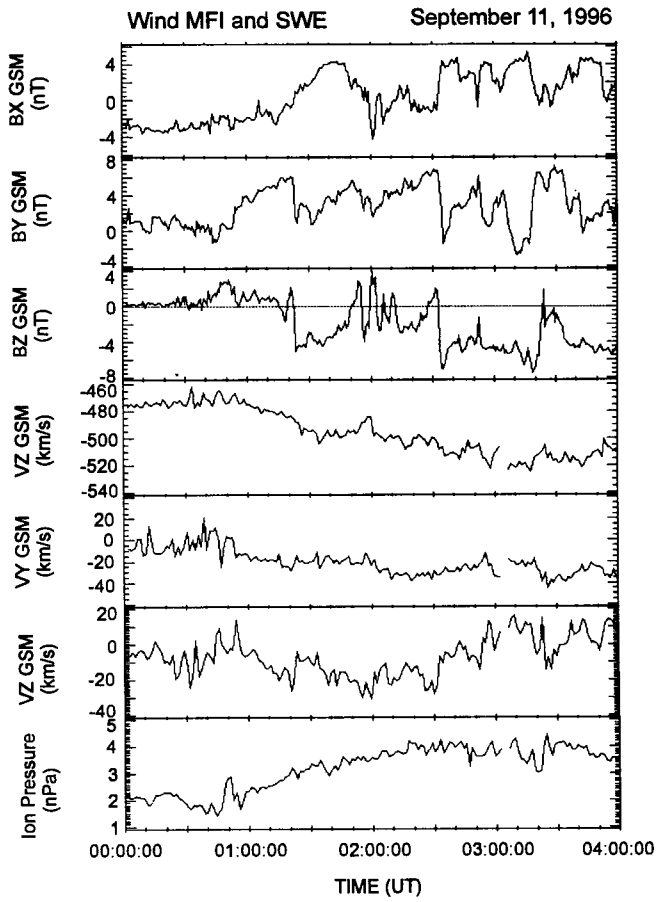

Fig 7. Four-hour plot of the IMF and solar wind parameters from the Wind spacecraft during the same time as the Polar TBL crossing as in Fig. 6. Plotted are the 3 components of the IMF in the GSM coordinate system, followed by the 3 components of the solar wind speed in the same coordinate system, and the ion pressure.

at ~ 01:00 UT, as noted by the onset of noisiness in the magnetic field (panel 4 of Fig.6) and an increase in density to about 10 cm^{-3} (panel 1 of Fig. 6) on Polar, the solar wind flow speed at Wind begins to increase in all 3 components. Likewise, the ion pressure (panel 7) begins to rise, the latter from about 2.5 to 4.0 nPa. Although these pressures are low, the increase appears to be tied to the onset of the TBL at Polar. It would thus appear that the magnetopause current layer has been compressed further into the cusp such that Polar crossed that boundary sheet on or around 00:45 UT, when a pressure pulse of about 1.5 nPa was measured at Wind, and entered the TBL. It seems possible that had this change in the solar wind not occurred, Polar would have remained in the cusp inside the magnetopause current layer and not encountered the TBL since its radial distance was decreasing for the entire interval of time. Polar exits the TBL at about the same time as the solar wind speed and pressure decrease around 03:40 UT.

In panels 1-3 of Fig. 7 we show the 3 components of the IMF in GSM coordinates as well as total field as measured by Wind. At around 01:23 UT, the IMF takes a sudden turn southward to around -5 nT. At precisely this time (see Fig. 6), the Hydra instrument on Polar begins to detect a

significant increase in the flux of anti field-aligned electrons around 1 keV, and anti field-aligned ions at energies .1 to 10 keV/e, increases in the fluxes of electrons with energies of a few eV and a broad range of keV ions perpendicular to **B**, and an increase in the intensity of the electromagnetic turbulence as seen in panel 4 by the MCA. A few minutes before (at ~01:18 UT) the IMF briefly turned south and these same effects are seen at that time for a brief period. Further changes in the IMF Z_{GSM} component at Wind throughout the TBL interval are definitely correlated with the effects just mentioned at Polar. All of these southward IMF related effects at Polar disappear as soon as the IMF turns sharply northward at ~ 03:22 UT, and as stated earlier, Polar exits the TBL when the solar wind pressure and speed drop, and no further effects are seen even though the IMF turned southward again. The plasma beta measured at Polar (pane 2 of Fig. 6) appears to show no correlation with IMF direction.

4 Discussion

The Polar wave measurements discussed in Sect. 3.1 appear to confirm that most of the electromagnetic turbulence observed by the LFWR in the frequency range 1-25 Hz is confined to the frequency range below f_{LH} and may be associated with waves propagating at wave normal angles closer to 90 degrees rather than 0 degrees, as would be expected for turbulence generated through the Lower Hybrid Drift Instability (LHDI). The primary waves seen from f_{LH} to 25 Hz occur at almost 2 f_{LH} and well below f_{ce}, are oscillatory and right-hand polarized and are probably whistler mode, although we do not rule out the possibility that these waves could be Doppler shifted lower hybrid waves. Due to the uncertainty in k as discussed in Sect. 3.1, the Doppler shift could be expected to lie in the range of 0.3 to ~60 Hz ($\omega_D = kV_{sat}$, where V_{sat} is the satellite velocity of ~2km/s and k was estimated to lie between 1.45×10^{-4} and $2.92 \times 10^{-2} m^{-1}$. Based on Figs. 6 and 7 we would like to stress that the level of turbulence appears to be higher under southward IMF which was mentioned by Vetoulis and Drake (1999) as evidence against LHDI for creating the turbulence. Furthermore, the electromagnetic turbulence seems to peak during steep gradients in the local magnetic field (see Fig. 4) and the electrostatic turbulence appears to occur during density gradients, which would favor a mechanism other than the LHDI.

Klimov et al. (1986) also report electromagnetic turbulence in the vicinity of the lower hybrid frequency from Prognoz-10 wave observations at the magnetopause. They suggest that the presence of the magnetic component together with the fact that the frequency of the emission is lower than the lower hybrid frequency (20 Hz) indicate that there is a magnetosonic nature to the waves. It is possible that fast magnetosonic waves are a candidate for creating the turbulence because they propagate perpendicular to the magnetic field, as is the case with the 1-10 Hz electromagnetic emissions observed by Polar. In addition magnetosonic waves possess both transverse and longitudinal components, are compressional, and can steepen and form shocks.

In the whistler mode frequency range of f_{LH} (typically 10-23 Hz) to f_{ce} (typically ~400 -1000 Hz in this magnetopause region), it does appear as if there is a tendency for the wave activity to be more intense for southward IMF than northward (see Fig.6). As mentioned above, various whistler mode waves are observed throughout the TBL, as are large gradients in the DC magnetic field. These observations suggest the strong possibility that the electromagnetic turbulence in the frequency range f_{LH} to f_{ce} is generated through the destabilization of whistler-like modes through the cross-field gradient of the field-aligned current (Drake et al., 1994a,b; Veloulis and Drake, 1999).

We also suggest the possibility that Alfvén waves may be present together with electromagnetic lower hybrid and whistler mode turbulence. Scudder et al. (1999) have recently analyzed a similar TBL region using Polar Hydra, MFE and Electric Field Instrument (EFI) data. They used the generalized Walén test to locate 44 rotational discontinuities or Alfvén wave trains within and across the current carrying layers of these structures at the magnetopause.

5 Conclusions

We conclude that a very turbulent boundary layer exists in the region just outside or near the cusp magnetopause current sheet in which various nonlinear processes are occurring. The TBL is characterized best by its electromagnetic turbulence that spans the frequency range from at least as low as 1 Hz, the lowest frequency resolved by PWI, to f_{ce}, typically several hundred Hz to 1-2 kHz. Analysis of this turbulence in the 1-10 Hz frequency range shows that the waves associated with it are propagating at angles close to 90° to **B** and at indices of refraction that fall between the theoretical values of the electromagnetic lower hybrid and whistler modes. Based upon the above discussion, the probability is strong that lower hybrid turbulence, and perhaps magnetosonic shock waves and Alfvén waves, and whistler mode turbulence are all present in the TBL region. We will have a better picture of this once we thoroughly analyze our data at the higher frequencies (20 Hz - 25 kHz). Thejappa et al. (1995b) have come to the same conclusion with regard to electromagnetic turbulence observed downstream of interplanetary shocks. Both the electromagnetic lower hybrid waves and whistlers fit the observed index of refraction. Both are Landau damped and must be generated locally, perhaps when the strong disturbances in the ambient magnetic field generate anisotropies in the local thermal plasma. In addition, Zhu et al. (1996) suggested that a plausible interpretation of the ISEE-1 data obtained at the magnetopause and analyzed by them is that there is a mixture of waves (whistler mode, lower hybrid and Alfvén) at the magnetopause.

Our correlation of the Polar wave data with Polar particle and field data and Wind solar wind and IMF data leads us to

conclude the following with respect to the TBL: 1) the electromagnetic turbulence in the range of 1 Hz up to f_{ce} is more intense during southward IMF, 2) the magnetopause current sheet may be compressed farther down into the cusp during increased solar wind pressure, 3) the DC magnetic field is depressed and noisy and the density is increased to 10 cm^{-3} or greater in the TBL, 4) both the electron and ion fluxes become anisotropic under southward IMF, 5) electrons around a few hundred eV become strongly opposed, and ion fluxes at several keV/e become opposed to the direction of the local magnetic field under southward IMF, and 6) the plasma beta is generally in the range of 1-10, which is more indicative of a magnetosheath plasma than a magnetospheric plasma at 8-9 R_E.

It is likely that the low-frequency turbulence (1 to ~ 10 Hz) may accelerate electrons on the order of a few hundred eV along the field lines according to the mechanism proposed by Vaĭsberg et al. (1983) or Vinas et al. (1997) for example. The Hydra electron data at these energies show that these particles are quite strongly aligned with the local magnetic field during times when the turbulence is present. Most of the other effects observed in the Polar particle data appear to be more strongly related to solar wind and IMF changes.

Acknowledgments. This study was carried out under Contract NAS5-30371 and Grants NAG5-7943 and NAG5-2231 with NASA/Goddard Space Flight Center. The authors would like to acknowledge Dr. C. T. Russell for use of the Polar MFE data; Dr. F. S. Mozer for use of the Polar EFI data; Dr. K. Ogilvie and the SWE Team for use of the Wind/SWE data; Dr. R. Lepping for use of the Wind/MFI data; Dr. C. Torrence and Dr. G. P. Compo of the University of Colorado for the use of their interactive Web software for creating the wavelet plot; NASA/GSFC for the use of the CDA Web plotting software; and Dr. R. Friedel of LANL and the Polar Hydra programming team at Iowa for developing the Papco plotting package, which was used to create many of the multi-instrument and multi-panel plots contained in this paper.

References

Acuña, M. H., Ogilvie, K. W., Baker, D. N., Curtis, S. A., Fairfield, D. H., and Mish, W. H., The Global Geospace Science Program and its investigations, *Space Sci. Rev.*, *71*, 5-21, 1995.

Blecki, J., Rothkaehl, H., Kossacki, K., Wronowski, R., Klos, Z., Juchniewicz, J., Savin, S., Romanov, S., Klimov, S., Triska, P., Smilaer, J., Simunek, J., Kudela, K., and Forster, M., ULF-ELF-VLF-HF plasma wave observations in the polar cusp onboard high and low altitude satellites, in *New Perspectives of collective effects: Proceedings of the International Topical Conference on Plasma Physics: Trieste, Italy, November 10-14, 1997*, P. K. Shukla, L. Stenflo, and R. Bingham, eds., *Physica Scripta Topical Volume T75*, 159-264, Royal Swedish Academy of Sciences, Stockholm, Sweden, 1998.

Cattell, C. A., Dombeck, J., Wygant, J. R., Hudson, M. K., Mozer, F. S., Temerin, M. A., Peterson, W. K., Kletzing, C. A., Russell, C. T., and Pfaff, R. F., Comparisons of Polar satellite observations of solitary wave velocities in the plasma sheet boundary and the high altitude cusp to those in the auroral zone, *Geophys. Res. Lett.*, *26*, 425-428, 1999.

Drake, J. F., Kleva, R. G., and Mandt, M. E., Structure of Thin Current Layers: Implications for Magnetic reconnection, *Phys. Rev. Lett.*, *73*, 1251-1254, 1994a.

Drake, J. F., Gerber, J., and Kleva, R. G., Turbulence and transport in the magnetopause current layer, *J. Geophys. Res.*, *99*, 11,211-11,223, 1994b.

Franz, J. R., Kintner, P. M., and Pickett, J. S., POLAR Observations of Coherent Electric Field Structures, *Geophys. Res. Lett.*, *25*, 1277-1280, 1998.

Gurnett, D. A. and Frank, L. A., Plasma Waves in the Polar Cusp: Observations from Hawkeye I, *J. Geophys. Res.*, *83*, 1447-1462, 1978.

Gurnett, D. A., Anderson, R. R., Tsurutani, B. T., Smith, E. J., Paschmann, G., Haerendel, G., Bame, S. J, and Russell, C. T., Plasma wave turbulence at the magnetopause: Observations from ISEE 1 and 2, *J. Geophys. Res.*, *84*, 7043-7058, 1979.

Gurnett, D. A., Persoon, A. M., Randall, R. F., Odem, D. L., Remington, S. L., Averkamp, T. F., DeBower, M. M., Hospodarsky, G. B., Huff, R. L., Kirchner, D. L., Mitchell, M. A., Pham, B. T., Phillips, J. R., Schintler, W. J., Sheyko, P., and Tomash, D. R., The Polar Plasma Wave Instrument, *Space Sci. Rev.*, *71*, 597-622, 1995.

Haerendel, G. and Paschmann, G., Entry of solar wind plasma into the magnetosphere, in *Physics of the hot plasma in the magnetosphere*, B. Hultqvist and L. Stenflo, eds., 23-43, Plenum Press, New York, 1975.

Harvey, P., Mozer, F. S., Pankow, D., Wygant, J., Maynard, N. C., Singer, H., Sullivan, W., Anderson, P. B., Pfaff, R., Aggson, T., Pedersen, A., Fälthammar, C.-G, and Tanskannen, P., The Electric Field Instrument on the Polar satellite, *Space Sci. Rev.*, *71*, 583-596, 1995.

Klimov, S. I., Nozdrachev, M. N., Triska, P., Voita, Ya., Galeev, A. A., Aleksevich, Ya. N., Afanas'ev, Yu., V., Baskakov, V. E., Bobkov, Yu. N., Dunets, R. B., Zhdanov, A. M., Korepanov, V. E., Romanov, S. A., Savin, S. P., Sokolov, A. Yu., and Shmelev, V. S., Plasma waves using the BUDVAR complex for combined wave diagnostics (Prognoz-10-Interkosmos), *Cosmic Research* (English translation), *24*, 143-149, *Kosmicheskie Issledovaniya* (original Russian), *24*, 177-184, 1986.

LaBelle, J. and Treumann, R. A., Plasma waves at the dayside magnetopause, *Space Sci. Rev.*, *47*, 175-202, 1988.

Pedersen, A., Solar wind and magnetospheric plasma diagnostics by spacecraft electrostatic potential measurements, *Ann. Geophys.*, *13*, 118-129, 1995.

Pickett, J. S., Gurnett, D. A., Menietti, J. D., LeDocq, M. J., Scudder, J. D., Frank, L. A., Sigwarth, J. B., Ackerson, K. L., Morgan, D. D., Franz, J. R., Kintner, P. M., Tsurutani, B. T., Ho, C. M., Chen, J., Fritz, T. A., Russell, C. K., Kasahara, Y., Kimura, I., Watanabe, S., Arkos, G. G., Rostoker, G., Kokubun, S., S., Fukunishi, H., Pfaff, R. F., Mozer, F. S., Hsieh, S.-Y., Mukai, T., and Chandler, M. O., Plasma waves observed during cusp energetic particle events and their correlation with Polar and Akebono satellite and ground data, *Adv. Space Res.*, *in press*, 1999.

Pottelette, R. and Treumann, R. A., Impulsive broadband electrostatic noise in the cleft: A signature of dayside reconnection, *J. Geophys. Res.*, *103*, 9299-9307, 1998.

Russell, C. T., Snare, R. C., Means, J. D., Pierce, D., Dearborn, D., Larson, M., Bar, G., and Le; G., The GGS/Polar Magnetic Fields Investigation, *Space Sci. Rev.*, *71*, 563-582, 1995.

Savin, S. P., Borodkova, N. L., Budnik, E. Yu., Fedorov, A. O., Klimov, S. I., Nozdrachev, M. N., Morozova, I. E., Nikolaeva, N. S., Petrukovich, A. A., Pissarenko, N. F., Prokhorenko, V. I., Romanov, S. A., Skalsky, A. A., Yermolaev, Yu. I., Zastenker, G. N., Zelenyi, L. M., Triska, P., Amata, E., Blecki, J., Juchniewicz, J., Buechner, J., Ciobanu, M., Grard, R., Haerendel, G., Korepanov, V. E., Lundin, R., Sandahl, I., Eklund, U., Nemecek, Z., Safrankova, J., Sauvand, J. A., Rustenbach, J., and Rauch, J. L., Interball Tail Probe measurements in outer cusp and boundary layers, in *Geospace Mass and Energy Flow: Results from the International Solar-Terrestrial Physics Program*, J. L. Horwitz, D. L. Gallagher, and W. K. Peterson, eds., *Geophysical Monograph 104*, 25-44, American Geophysical Union, Washington, D.C., 1998.

Scudder, J., Hunsacker, F., Miller, G., Lobell, J., Zawistowski, T., Ogilvie, K., Keller, J., Chornay, D., Herrero, F., Fitzenreiter, R., Fairfield, D., Needell, J., Bodet, D., Googins, J., Kletzing, C., Torbert, R., Vandiver, J., Bentley, R., Fillius, W., McIlwain, C., Wipple, E., and Korth, A., Hydra - A 3-dimensional electron and ion hot plasma instrument for the Polar spacecraft of the GGS mission, *Space Sci. Rev.*, *71*, 459-495, 1995.

Scudder, J. D., Puhl-Quinn, P., Mozer, F. S., Ogilvie, K. W., and Russell, C. T., Generalized Walen tests through Alfven waves and rotational discontinuities using electron flow vortices, *J. Geophys. Res.*, *in press*, 1999.

Sonnerup, B. U. O. and Cahill, L. J., Jr., Magnetopause structure and attitude from Explorer 12 observations, *J. Geophys. Res.*, *72*, 171-183, 1967.

Thejappa, G., Wentzel, D. G., and Stone, R. G., Low-frequency waves associated with Langmuir waves in solar wind, *J. Geophys. Res.*, *100*, 3417-3426, 1995a.

Thejappa, G., Wentzel, D. G., MacDowall, R. J., and Stone, R. G., Unusual wave phenomena near interplanetary shocks at high latitudes, *Geophys. Res. Lett.*, *22*, 3421-3424, 1995b.

Torrence, C. and Compo, G. P., A practical guide to wavelet analysis, *Bull. Amer. Meteor. Soc.*, *79*, 61-79, 1998.

Tsurutani, B. T., Lakhina, G. S., Ho, C. M., Arballo, J. K., Galvan, C., Boonsiriseth, A., Pickett, J. S., Gurnett, D. A., Peterson, W. K., and Thorne, R. M., Broadband plasma waves observed in the polar cap boundary layer: Polar, *J. Geophys. Res.*, *103*, 17,351-17,366, 1998.

Vaĭsberg, D. L., Galeev, A. A., Zastenker, G. N., Klimov, S. I., Nozdracheve, M. N., Sagdeev, R. Z., Sokolov, A. Yu., and Shapiro, V. D., Electron acceleration in the front of a strong collisionless shock wave, *Sov. Phys. JETP (English Trans.)*, *58*, 716-721, *Zh. Eksp. Teor. Fiz (Original Russian)*, *85*, 1232-1243, 1983.

Vetoulis, G. and Drake, J. F., Whistler turbulence at the magnetopause 1. Reduced equations and linear theory, *J. Geophys. Res.*, *104*, 6919-6928, 1999.

Vinas, A. F., Goldstein, M. L., and Wong, H. K., Parallel electric fields associated with low frequency MHD waves, *EOS, Transactions, American Geophysical Union*, *78*, F558, 1997.

Zhu, Z., Song, P., Drake, J. F., Russell, C. T., Anderson, R. R., Gurnett, D. A., Ogilvie, K. W., and Fitzenreiter, R. J., The relationship between ELF-VHF waves and magnetic shear at the dayside magnetopause, *Geophys. Res. Lett.*, *23*, 773-776, 1996.